



OPEN

Fine tuning of graphene-metal adhesion by surface alloying

SUBJECT AREAS:

GRAPHENE

SYNTHESIS OF GRAPHENE

MECHANICAL AND STRUCTURAL
PROPERTIES AND DEVICES

STRUCTURAL PROPERTIES

Received

13 June 2013

Accepted

29 July 2013

Published

13 August 2013

Correspondence and
requests for materials
should be addressed to
A.B. (alessandro.
baraldi@elettra.trieste.it)

D. Alfè^{1,2}, M. Pozzo¹, E. Miniussi^{3,4}, S. Günther⁵, P. Lacovig⁶, S. Lizzit⁶, R. Larciprete⁷, B. Santos Burgos⁶, T. O. Mendes⁶, A. Locatelli⁶ & A. Baraldi^{3,4}

¹Department of Earth Sciences, Department of Physics and Astronomy, TYC@UCL, and London Centre for Nanotechnology, University College London, Gower Street, London WC1E 6BT, United Kingdom, ²IOM-CNR, DEMOCRITOS National Simulation Centre, I-34100 Trieste, Italy, ³Physics Department and CENMAT, University of Trieste, Via Valerio 2, I-34127 Trieste, ITALY, ⁴IOM-CNR, Laboratorio TASC, S.S. 14 Km 163.5, I-34149 Trieste, ITALY, ⁵Technische Universität München, Chemie Department, Physikalische Chemie mit Schwerpunkt Katalyse, Lichtenbergstr. 4, D-85748 Garching, Germany, ⁶Elettra - Sincrotrone Trieste S.C.p.a., S.S. 14 Km 163.5, 34149 Trieste, ITALY, ⁷CNR-Institute for Complex Systems, via Fosso del Cavaliere 100, I-00133 Roma, Italy.

We show that bimetallic surface alloying provides a viable route for governing the interaction between graphene and metal through the selective choice of the elemental composition of the surface alloy. This concept is illustrated by an experimental and theoretical characterization of the properties of graphene on a model PtRu surface alloy on Ru(0001), with a concentration of Pt atoms in the first layer between 0 and 50%. The progressive increase of the Pt content determines the gradual detachment of graphene from the substrate, which results from the modification of the carbon orbital hybridization promoted by Pt. Alloying is also found to affect the morphology of graphene, which is strongly corrugated on bare Ru, but becomes flat at a Pt coverage of 50%. The method here proposed can be readily extended to several supports, thus opening the way to the conformal growth of graphene on metals and to a full tunability of the graphene-substrate interaction.

It is well known that the coupling between supported graphene (GR) and the substrate is responsible for a number of properties of GR-based materials, including the electromechanical properties¹, contact resistance², work function³, and ultrastrong adhesion⁴, as well as the electronic^{5–10} and heat transport properties¹¹. Several methods, such as the choice of the substrate¹², the intercalation of adspecies^{13–18}, or the creation of an oxide buffer layer¹⁹, have been proven to be a possible means of controlling the graphene-metal interaction, though not *ad libitum*. These approaches, in fact, do not enable to precisely control the graphene-substrate coupling strength and come with some significant drawbacks. For instance, the penetration of adsorbates between graphene and the substrate requires layer defects to allow intercalation and results in the formation of a non-uniform interface.

We here propose surface alloying as a novel, alternative approach to tailor the GR-substrate interaction to any desired extent. To prove this concept, we grew graphene on a PtRu surface alloy with a variable Pt content. Fig. 1 schematically illustrates our experimental design. Starting from a clean Ru(0001) surface (Fig. 1 (a)), we deposited a variable amount (≤ 0.5 ML) of Pt on the substrate (Fig. 1 (b)) and annealed the sample to 1300 K in order to promote the intermixing of the two metal species in the top layer (Fig. 1 (c)). As demonstrated by previous studies²⁰, the so obtained PtRu surface alloy exhibits a random distribution of the Pt atoms, which are confined to the first layer. Graphene was subsequently grown by ethylene chemical vapour deposition (CVD) (Fig. 1 (d)), which is a commonly used procedure for the production of large scale graphene. In the present case, a temperature of 1050 K and an ethylene pressure in the range $1 \times 10^{-9} \div 1 \times 10^{-7}$ mbar allowed obtaining an extended, well-ordered graphene layer whose interaction with the substrate directly depends on the concentration of Pt atoms.

Results

We first investigated the growth mechanisms and morphology of GR on clean Ru(0001), which represents our reference system. Low Energy Electron Microscopy (LEEM) images acquired during C₂H₄ chemical vapour deposition (CVD) at T = 1020 K show that GR grows in a continuous, rolling-carpet fashion (Fig. 2 (a)), in agreement with previous studies^{21,22}. The Low Energy Electron Diffraction (LEED) pattern of single-layer GR/Ru(0001) shows the periodicity of a moiré superlattice, formed by (13 × 13) unit cells of GR over (12 × 12) substrate unit cells, in good agreement with the results of higher resolution surface x-ray diffraction

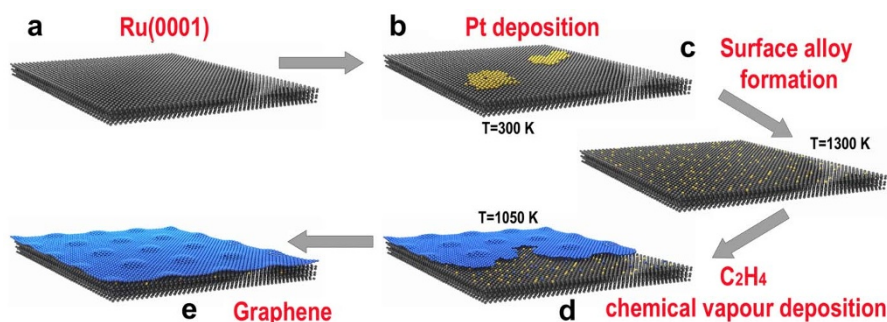


Figure 1 | Schematic illustration of our experimental design for graphene growth on a PtRu surface alloy. (a) The clean Ru(0001) single crystal. (b) Pt islands (yellow atoms) formed after room temperature deposition of a submonolayer amount of Pt on Ru(0001). (c) The PtRu surface alloy obtained by annealing the system to 1300 K to induce intermixing of the two metal species in the top layer. (d) GR growth on the PtRu surface alloy by ethylene CVD at 1050 K; the C layer starts growing along the substrate steps and subsequently extends to the terraces. (e) Extended, long range ordered GR layer on the PtRu surface alloy.

experiments²³. C 1s core level (CL) photoemission measurements performed during CVD (Fig. 2 (b)) show the development of two components, ascribed to populations of strongly (S) and weakly (W) interacting carbon atoms of the graphene layer²⁴, both increasing at a linear rate with a constant intensity ratio S:W of ~ 2.5 (Fig. 2 (c)). The two components are separated by 630 ± 20 meV, in agreement with

the value found for an extended GR layer on Ru(0001)^{19,24}. Density functional theory (DFT) calculations for GR/Ru(0001) (see Methods), performed with the VASP code²⁵ (Fig. 1 (d)), confirm that the GR layer is strongly buckled²⁶, with a corrugation of 1.55 \AA , and a minimum distance from the first Ru layer of 2.15 \AA . DFT allowed us to calculate the C 1s CL binding energy (BE) for each of the 338 C

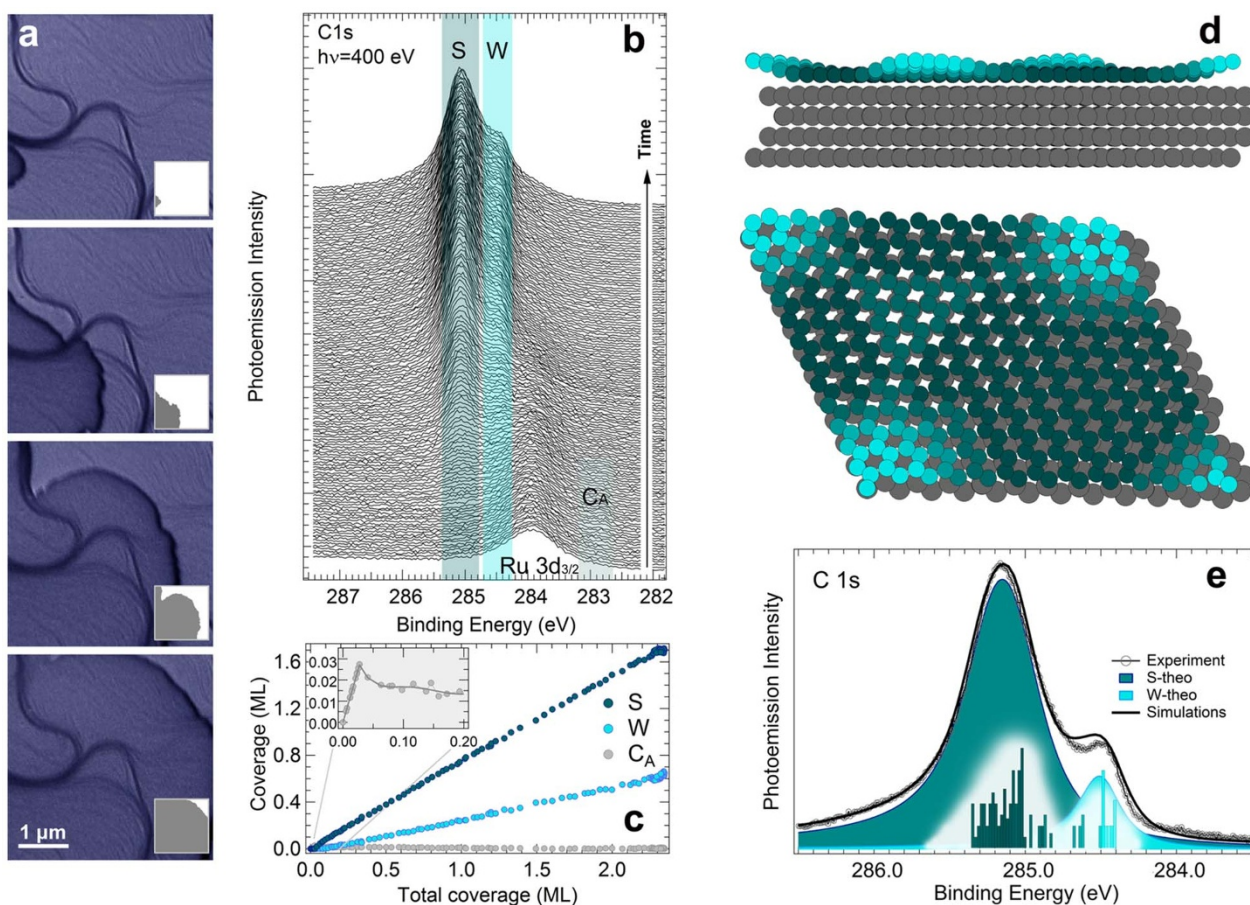


Figure 2 | Microscopic, spectroscopic and theoretical characterisation of Graphene on Ru(0001). (a) LEEM images of graphene growth on clean Ru(0001) by C_2H_4 exposure at $T = 1020 \text{ K}$ ($p(\text{C}_2\text{H}_4) = 2 \div 5 \times 10^{-8} \text{ mbar}$). In the inset is shown (in grey) the sample area already covered by graphene. (b) C 1s spectra during C_2H_4 exposure at $T = 1020 \text{ K}$. (c) Partial coverage of strongly (S) and weakly (W) interacting GR, and C monomers (C_A) as a function of the total C coverage. (d) Side and top view of the DFT-simulated moiré cell of GR/Ru(0001); the colour scale reflects the C-substrate distance. (e) Comparison between the experimental C 1s spectrum of GR and the calculated spectral distribution. The decomposition of the theoretical spectrum into strongly (S-theo) and weakly (W-theo) interacting components is also shown superimposed, along with the histogram of the calculated BE distribution.



atoms of the moiré cell. The experimental spectrum was subsequently fitted to a sum of 338 Doniach-Šunjić functions²⁷ convoluted with a Gaussian, holding the BEs fixed to the DFT-calculated values. The simulated spectral distribution (Fig. 2 (e)) shows that the two main components actually arise from a continuous distribution of non-equivalent C atomic configurations, thus proving the power of our approach³⁹ in distinguishing regions of the moiré cells with different degrees of C-substrate interaction. As carbon is deposited on the Ru(0001) surface, another C species (C_A in Fig. 2 (b)–(c)), which shows up as a small shoulder at 282.82 eV BE, is initially detected before the appearance of GR. This species, which reaches a maximum coverage of ~ 0.03 ML (see inset in Fig. 2 (f)), eventually disappears as GR starts nucleating, with both S and W growing at the expenses of C_A . Notice that we adopt the definition of one monolayer as the coverage yielding one adsorbate for each atom of the substrate surface.

In order to accurately determine the nature of C_A , we calculated the adsorption energies and C 1s CL BEs of a number of selected C adatoms and dimers adsorbed in non-equivalent configurations, both on the terraces and at the (100) and (111) steps of Ru(0001). We found that the threefold hcp site on the terraces (M_{H1}) and the C monomer at the steps (M_{F2}) have very similar adsorption energies (Fig. 3 (a)), thus confirming that, at the typical GR growth temperatures, substrate steps do not act as efficient C monomer trapping centres²⁸. A comparison between the calculated C 1s BEs and the experimental spectrum (Fig. 3 (c)), provides direct spectroscopic evidence that the species named C_A is the C monomer adsorbed at hcp sites on the atomic terraces. As first pointed out by Loginova

*et al.*²¹, these monomers form a 2D lattice gas which supplies C atoms for GR formation. In the theoretical model of Chen *et al.*²⁸, GR growth then proceeds through the migration of C monomers to the steps, where dimerization is energetically favoured ($D_{A1} - D_{A2}$, $D_{B1} - D_{B2}$), and through the subsequent attachment of C atoms.

After this preliminary characterization, we prepared the PtRu surface alloy following a well-established method²⁰. The so obtained surface alloy is thermally stable above the typical growth temperature of GR, and shows a random distribution of the Pt atoms in the first layer up to a Pt concentration of 80%. The intermixing between the two metals is confined to the first layer of the system, and does not modify the surface lattice parameter with respect to that of clean Ru(0001).

The first difference between Ru(0001) and the PtRu alloy is the GR growth mechanism. At a Pt concentration of 0.5 ± 0.1 ML, LEEM images (Fig. 4 (a)) show that GR first nucleates and grows along the step edges. Only at a later stage, when the number of available sites at the steps has significantly decreased, the GR islands extend to the terraces. The LEED data show that the periodicity of the moiré cell on the PtRu alloy is the same as that of GR/Ru(0001) (see Supplementary Data).

Following the same procedure used for GR/Ru(0001), the evolution of the C 1s spectra during C_2H_4 CVD was monitored for various initial Pt concentrations. In this case, the coverage-dependent behaviour of the S and W C 1s components, is remarkably different from what observed on clean Ru(0001). At low Pt content (0.12 ML, Fig. 4 (b)), the two peaks grow linearly up to a C coverage of ~ 2 ML,

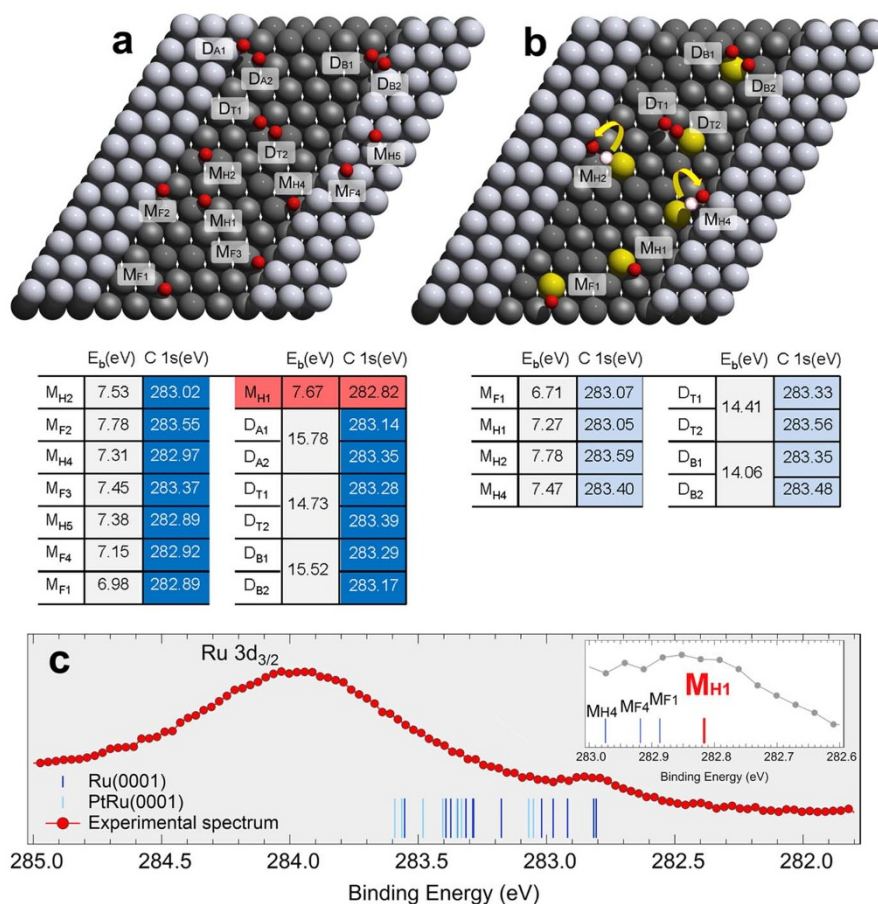


Figure 3 | Density Functional Theory description of the different carbon surface species. (a–b) DFT-simulated cells for C adsorption on Ru(0001) and on the PtRu surface alloy, respectively (yellow = Pt; red = C). The corresponding adsorption energies (E_b) and C 1s CL BEs are reported in the tables. (c) Comparison between the experimental C 1s CL spectrum (red points) and the calculated BE distributions for C adsorption on Ru(0001) and on PtRu (blue and light blue bars, respectively).

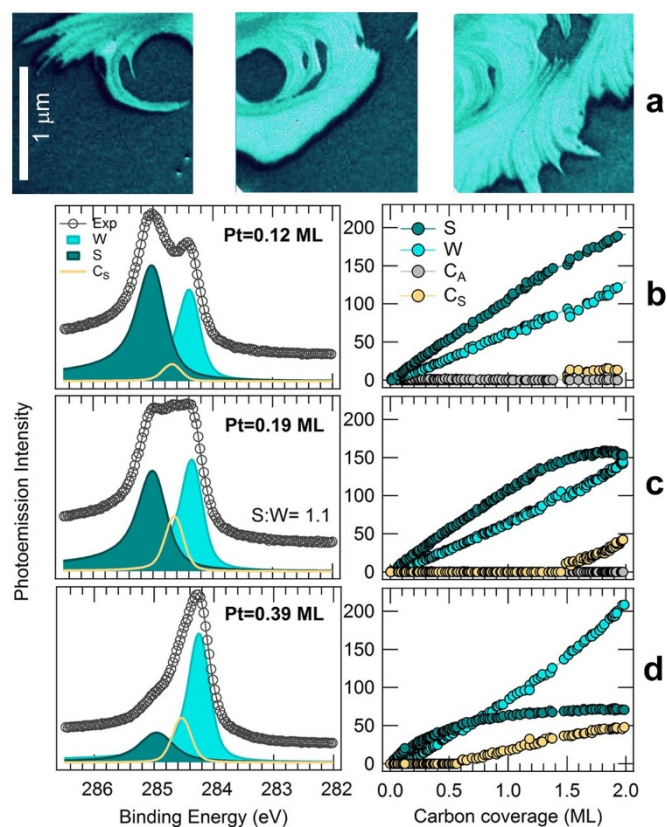


Figure 4 | Microscopic and spectroscopic characterization of Graphene grown on different PtRu surface alloys. (a) LEEM images of GR growth on the PtRu surface alloy (Pt coverage = 0.5 ± 0.1 ML) by C_2H_4 CVD at $T = 1020$ K. The brighter areas correspond to GR-covered regions of the substrate, while the darker ones indicate clean areas of the sample. (b–d) $C1s$ spectra at ~ 2 ML C coverage (after subtraction of the $Ru3d_{3/2}$ signal), and their deconvolution into S, W and second-layer (C_S) GR components; intensity evolution of the $C1s$ photoemission intensities of the various C species during C_2H_4 exposure. The reported S:W intensity ratios were calculated at 2 ML C coverage.

keeping a nearly constant ratio ($S : W \approx 1 : 5$). At higher Pt concentrations (0.19 and 0.39 ML, Fig. 5 (c)–(d)), instead, we observe a net deviation from the linear regime: the S:W ratio, which is initially skewed towards the strongly interacting component, evolves in favour of W as the C coverage increases, reaching a value of 1.1 and 0.35 at 2 ML coverage. These results prove that the selective tuning of the Pt concentration in the binary alloy enables modifying the number of strongly and weakly interacting C atoms in the moiré cell of GR.

Also in this case, we detect a small $C1s$ component at about 282 eV BE in the initial stage of GR growth, although it is significantly weaker than on Ru(0001), and becomes experimentally indistinguishable at 0.39 ML Pt. At high Pt coverage and for larger C_2H_4 exposures, we also observe the appearance of a third $C1s$ component (C_S in Fig. 4) at 284.65 eV BE. We identified this species as a multilayer GR structure, based on the similarity with the BE of the GR multilayer component identified on Ru(0001) (see Supplementary Information). This interpretation is further supported by low energy electron reflectivity measurements contrast²⁹, which locally indicate the presence of multilayer GR patches on the substrate.

DFT allowed us to gain further insight into the morphology, electronic structure and growth mechanisms of GR on the PtRu surface alloy. We first modelled a surface cell assuming no Pt at the step edges and a random distribution of the Pt atoms in the first layer (as

suggested by previous STM works²⁰) (Fig. 3 (b)), and we calculated the adsorption energies and $C1s$ core level BEs of the C monomers and dimers in each adsorption configuration. The results clearly indicate that the Pt atoms in the PtRu alloy weaken the C-metal bonding for both monomers and dimers. Moreover, the higher concentration of Ru atoms at the steps induces a preferential migration of the C adatoms from the terraces to the steps, where they bind to Ru, and hence allow GR nucleation. Our simulations, in fact, show that, if a C adatom is initially placed next to a Pt atom on a terrace, it will spontaneously move to the nearest step site after relaxation (see M_{H_2} and M_{H_4} in Fig. 3 (b)). As the C coverage increases, GR extends also to the terraces; at this stage, the faster growth rate of W with respect to S eventually leads to a crossover between the intensity curves of the two species.

We then carried out a set of DFT calculations for GR on PtRu, at Pt concentrations of 0.1, 0.2 and 0.5 ML. It turns out that both the morphology and the electronic structure of GR strongly depend on the amount of Pt, and that the C layer is sensitive not only to the density, but also to the spatial distribution of the Pt atoms in the first layer. The main consequence is the local detachment of the C layer (from 2.15 Å on clean Ru surface to 3.95 Å at 0.5 ML) in the regions of the moiré cell overlying Pt atoms (Fig. 5). The changes caused by Pt atom deposition are especially evident in the differences between the charge distributions obtained by putting a completely decoupled graphene layer in contact with the Ru(0001) and with the PtRu surface (Fig. 5 (b)). For GR on Ru(0001), the chemical interaction with the substrate induces a charge redistribution in the buckled regions of the moiré cell. By contrast, the introduction of Pt atoms in the first layer results in the formation of small GR areas where the charge density distribution is comparable to that of a GR layer that has been completely decoupled from the substrate, thus indicating a significantly reduced interaction and a limited orbital rehybridization. The effect of the presence of Pt atoms underneath the carbon layer on the GR-metal adhesion can be appreciated in the side view of the charge redistribution (Fig. 5 (b)). Finally, as we did for GR/Ru(0001), we calculated the $C1s$ BEs for each atom in the cell, at various Pt coverages. A comparison of the simulated spectral distributions (Fig. 5 (c)) clearly shows that the intensity ratio S:W decreases as the Pt concentration in the first layer increases, a trend which faithfully reproduces our experimental observations. Therefore, the larger amount of Pt atoms in the first layer of the alloy leads to a progressive detachment of the C layer from the metal substrate.

Discussion

Although it is widely accepted that graphene interacts weakly with Pt(111) and strongly with Ru(0001)^{12,24}, it is not straightforward to conclude that the presence of Pt in a surface alloy directly weakens the graphene-substrate interaction, and that an increased concentration of randomly distributed guest atoms in the first layer automatically reduces the GR adhesion to the substrate. In fact, the electronic structure of surface and/or near-surface alloys is always largely modified by ligand and strain effects.

The interpretation of our results can be found by using the d -band model which describes the link between adsorption energy and d -band centre³⁰. When the Pt atoms are embedded in a matrix of Ru atoms, the Pt-metal bonds are laterally compressed (2.71 Å) compared to the lattice constant of Pt(111) (2.77 Å). This compression would already induce a weakening of the interaction of any adsorbate with the substrate. In our system, the addition of Pt atoms causes a downshift of the surface projected d -band centre E_d of first-layer atoms with respect to the clean Ru(0001). More specifically, we find that E_d moves from 0.61 eV for bare Ru(0001), to 0.73, 0.84 and 1.20 eV for the surface alloy at Pt coverages of 0.1, 0.2 and 0.5 ML, respectively. These results prove that the d -band model can be extended to describe the trends in the GR-metal interaction, when

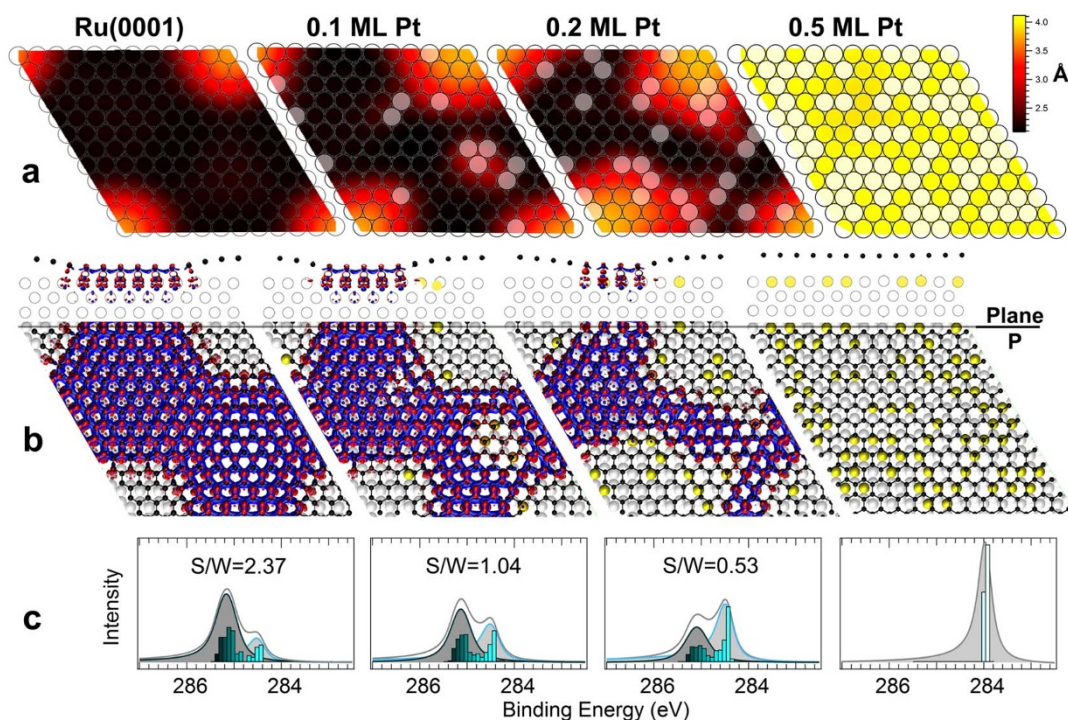


Figure 5 | Density Functional Theory explanation of the variable interaction of graphene grown on the PtRu surface alloy. (a) 2D plot of the simulated moiré cell of GR on the PtRu surface alloy, at various Pt concentrations. The colour scale indicates the C-metal distance. The first layer atoms of the substrate are shown superimposed, with the Pt atoms highlighted in a white shade. (b) Simulated difference map (top and side views) of the charge density of graphene on Ru(0001) and PtRu/Ru(0001), with respect to a completely decoupled GR layer on Ru(0001). Red and blue isosurfaces indicate charge accumulation and depletion regions, corresponding to an electron concentration of $\pm 0.023 \text{ e } \text{Å}^{-3}$, respectively. Side views: 2D projections of the charge difference map along the plane P normal to the surface plane. (c) DFT-simulated C 1s core level spectra of GR on the Ru and PtRu surfaces, and their deconvolution into strongly (S) and weakly (W) interacting GR components.

the lattice mismatch effects can be separated from the chemical effects. We can therefore expect that graphene on a full monolayer of Pt on Ru(0001) will be even more weakly bonded than a graphene layer on Pt(111).

The interplay between lattice mismatch and chemical effects has already been addressed in the case of strongly interacting graphene-substrate systems (as in the case of Ni(111) and Fe(110)³¹), for which the lattice mismatch has been shown to play a secondary role. Our experiments, on the other hand, prove that a similar trend applies also to the case of weakly interacting systems. More specifically, starting from a strongly coupled system like GR/Ru(0001) and gradually changing the chemical composition of the substrate while keeping the lattice constant unchanged (as for PtRu and Ru(0001)), the graphene interaction is significantly modified. Our findings hence provide direct evidence that the interaction strength is dominated by chemical effects rather than by the geometrical lattice mismatch between graphene and the substrate.

In conclusion, we have proven that a bimetallic surface alloy can be used to grow an extended and thermally stable high-quality graphene layer, whose interaction with the support can be selectively tuned by modifying the chemical composition of the first layer of the substrate. The modulation in the GR-substrate coupling can be described in terms of the *d*-band model.

The understanding of the physical mechanisms responsible for the different levels of adhesive interaction could be of impact to the fabrication and performance of devices based on graphene-metal junctions, and to the integration of graphene in hybrid two-dimensional structures. It will also potentially find use in surface protective coatings and high-power nanoelectronic applications for which a low thermal and electrical resistance are a fundamental requirement, along with a high thermal stability³².

Methods

Experimental methods. The photoemission experiments were performed at the SuperESCA beamline of the third-generation synchrotron radiation source Elettra in Trieste. The ultrahigh vacuum chamber (base pressure $\leq 2 \times 10^{-10}$ mbar) is equipped with standard surface science facilities for sample cleaning and characterization, and with a Phoibos hemispherical electron energy analyser from SPECS (mean radius of 150 mm), combined with a custom home-made delay-line detection system. The energy tunability and the high brilliance of synchrotron radiation allow monitoring in real time the evolution of the atomic core levels of the sample under reaction conditions. The overall experimental resolution attained in our experiments was of the order of 50 meV for the C 1s signal.

Low energy electron microscopy (LEEM) is a well-established technique used for imaging dynamic processes at surfaces and interfaces. It employs slow electrons to probe crystalline specimens, using backscattered electron for imaging surfaces. It can be used in bright- or dark-field mode, depending on whether primary or secondary diffracted beams are employed. The LEEM experiments presented in this work were carried out at the Nanospectroscopy beamline of the Elettra synchrotron radiation facility using the SPELEEM III microscope (Elmitec). This instrument combines low energy electron microscopy and diffraction with energy filtered X ray photoemission microscopy. The current lateral resolution is close to 10 nm in LEEM mode. The diffraction measurements are restricted to an area of about 2 μm in diameter.

The Ru(0001) crystal was cleaned by repeated cycles of Ar⁺ sputtering at 2.5 keV ($p(\text{Ar}) = 3 \times 10^{-6}$ mbar) and annealing to 1500 K, followed by a high temperature oxidizing treatment to remove bulk C contaminants ($p(\text{O}_2) = 5 \times 10^{-7}$ mbar; $550 < T < 1100$ K), and a reducing treatment in H₂ atmosphere to remove residual oxygen ($p(\text{H}_2) = 2 \times 10^{-7}$ mbar; $550 < T < 1500$ K). The C 1s, O 1s and S 2p CL spectra after this procedure show no evidence of residual contaminants. The PtRu surface alloy was prepared following the method developed by Diemant *et al.*³³.

A submonolayer amount of Pt was first deposited at room temperature on clean Ru(0001) using a Pt evaporator. Annealing the as deposited layer to 800 K results in the formation of Pt ad-islands covering the Ru(0001) surface, which appear as bright spots in the LEEM images. The grayscale contrast between the bright Pt-covered areas and the homogeneous Ru(0001) substrate in the background was exploited to estimate the amount of Pt deposited on the sample prior to alloying, using a particle analysis algorithm. More specifically, the border of the bright islands was first detected by differentiating the images in the *x* and *y* dimensions (the maximum gradient corresponding to edge regions), and the regions defined by the edges were then measured and compared with the total area of the image. In order to promote the



formation of a random alloy in the Ru(0001) surfaces with Pt atoms embedded in the first layer of Ru, we annealed the surface to 1300 K. The Pt islands visible after Pt deposition (see LEEM image in Supplementary Fig. S1 (a)) irreversibly disappear upon alloying (see Supplementary Fig. S1 online (b)). The surface at this stage shows a uniform contrast in LEEM, thus signifying a redistribution of the Pt atoms in the Ru surfaces, as previously demonstrated by extended STM experiments performed by the group of Behm³⁴.

In the photoemission experiments, the Pt coverage was estimated by comparing the intensities of the Pt $4f_{7/2}$ and of the Ru $3d_{5/2}$ signal, after normalizing them to the photon flux and to the photoelectron cross section. The Ru $3d_{5/2}$ photoemission intensity, which receives a contribution from both bulk and surface Ru atoms, was additionally rescaled to account for the depth-dependent signal attenuation due to the inelastic photoelectron mean free path in the crystal, as derived from the Tanuma, Powell, and Penn formula³⁵. The Pt $4f_{7/2}$ core level spectrum, acquired after Pt evaporation on the clean Ru(0001) substrate, both before and after annealing to 1300 K can be fitted to a single component ascribed to the surface alloy, which does not appreciably lose intensity upon annealing, thus ruling out Pt bulk dissolution at Pt coverages ≤ 0.5 ML.

Theoretical methods. The density functional theory (DFT) calculations have been performed with the VASP code²⁵, using PAW potentials³⁶ and the PBE exchange-correlation functional³⁷. Single particle orbitals were expanded in plane waves (PW), with a planewave kinetic energy cutoff of 400 eV. The lattice parameter of Ru was used to model both the Ru(0001) surface and the PtRu/Ru(0001) surface alloy. The adsorption of graphene on the Ru(0001) surface has been modelled by overlaying a (13×13) graphene sheet over a (12×12) Ru(0001) super-cell and using a slab of 5 Ru layers. In all the calculations the energy was minimized until the forces acting on the atoms were smaller than 0.01 eV/Å. A vacuum interspace of at least 10 Å was used to minimize the interaction between periodic images of the slab along the direction perpendicular to the surface, resulting in a supercell of 21.5 Å along the z axis. The SCLSs were calculated in the final state approximation as described in Ref. 25,38. We used the Γ point only to sample the Brillouin zone. Spot checks using a $2 \times 2 \times 1$ grid showed that with just the Γ point SCLS are converged to better than 5 meV. For the clean surface, we used up to 7 atomic layers, and the results show that with 5 or more layers the SCLS are converged to within ~ 10 meV. Charge density differences have been calculated as $n_{M-GR} - n_M - n_{GR}$, where n_{M-GR} is the total electronic charge density of the slab with GR adsorbed on top, n_M is the charge density of the isolated slab with exactly the same geometry and n_{GR} the charge of the GR layer, also in the same geometry as when adsorbed on the slab.

- Klimov, N. N. *et al.* Electromechanical properties of graphene drumheads. *Science* **336**, 1557–1561 (2012).
- Xia, F., Perebeinos, V., Lin, Y.-m., Wu, Y. & Avouris, P. The origins and limits of metal-graphene junction resistance. *Nat. Nanotech.* **6**, 179–193 (2011).
- Gong, C. *et al.* Metal-graphene-metal sandwich contacts for enhanced interface bonding and work function control. *ACS Nano* **6**, 5381–5387 (2012).
- Koenig, S. P., Boddeti, N. G., Dunn, M. L. & Bunch, J. S. Ultrastrong adhesion of graphene membranes. *Nat. Nanotech.* **6**, 543–546 (2011).
- Geim, A. K. & Novoselov, K. S. The rise of graphene. *Nature Mat.* **6**, 183–191 (2007).
- Zhou, S. Y. *et al.* Substrate-induced bandgap opening in epitaxial graphene. *Nature Mat.* **6**, 770–775 (2007).
- Ji, S.-H. *et al.* Atomic-scale transport in epitaxial graphene. *Nature Mat.* **11**, 114–119 (2012).
- Lee Eduardo, J. H., Balasubramanian, K., Weitz, R. T., Burghard, M. & Kern, K. Contact and edge effects in graphene devices. *Nature Nanotech.* **3**, 486–490 (2008).
- Giovannetti, G. *et al.* Doping graphene with metal contacts. *Phys. Rev. Lett.* **101**, 026803–026806 (2008).
- Adamska, L., Lin, Y., Ross, A. J., Batzill, M. & Oleynik, I. I. Atomic and electronic structure of simple metal/graphene and complex metal/graphene/metal interfaces. *Phys. Rev. B* **85**, 195443–195450 (2012).
- Balandin, A. A. Thermal properties of graphene and nanostructured carbon materials. *Nature Mat.* **10**, 569–581 (2011).
- Batzill, M. The surface science of graphene: Metal interfaces, cvd synthesis, nanoribbons, chemical modifications, and defects. *Surf. Sci. Rep.* **67**, 83–115 (2012).
- Riedl, C., Coletti, C., Iwasaki, T., Zakharov, A. A. & Starke, U. Quasi-free-standing epitaxial graphene on sic obtained by hydrogen intercalation. *Phys. Rev. Lett.* **103**, 246804–246807 (2009).
- Bostwick, A. *et al.* Observation of plasmarons in quasi-freestanding doped graphene. *Science* **328**, 999–1002 (2010).
- Sutter, P. W., Flege, J.-I. & Sutter, E. A. Epitaxial graphene on ruthenium. *Nature Mat.* **7**, 406–411 (2008).
- Shikin, A. M., Prudnikova, G. V., Adamchuk, V. K., Moresco, F. & Rieder, K.-H. Surface intercalation of gold underneath a graphite monolayer on Ni(111) studied by angle-resolved photoemission and high-resolution electron-energy-loss spectroscopy. *Phys. Rev. B* **62**, 13202–13208 (2000).
- Sutter, P., Sadowski, J. T. & Sutter, E. A. Chemistry under cover: tuning metal-graphene interaction by reactive intercalation. *J. Am. Chem. Soc.* **132**, 8175–8179 (2010).
- Larciprete, R. *et al.* Oxygen switching of the epitaxial graphene-metal interaction. *ACS Nano* **6**, 9551–9558 (2012).
- Lizzit, S. *et al.* Transfer-free electrical insulation of epitaxial graphene from its metal substrate. *Nano Lett.* **12**, 4503–4507 (2012).
- Hoster, H. E. *et al.* Pt_xRu_{1-x}/Ru(0001) surface alloys formation and atom distribution. *Phys. Chem. Chem. Phys.* **10**, 3812–3823 (2008).
- Loginova, E., Bartelt, N. C., Feibelman, P. J. & McCarty, K. F. Evidence for graphene growth by C cluster attachment. *New J. Phys.* **10**, 093026 (2008).
- Günther, S. *et al.* Single terrace growth of graphene on a metal surface. *Nano Lett.* **11**, 1895–1900 (2011).
- Martocchia, D. *et al.* Graphene on Ru(0001): A 25×25 supercell. *Phys. Rev. Lett.* **101**, 126102–126105 (2008).
- Preobrajenski, A. B., Ng, M. L., Vinogradov, A. S. & Mårtensson, N. Controlling graphene corrugation on lattice-mismatched substrates. *Phys. Rev. B* **78**, 073401–073404 (2008).
- Kresse, G. & Furthmüller, J. Efficiency of ab-initio total energy calculations for metals and semiconductors using a plane-wave basis set. *Comput. Mater. Sci.* **6**, 15–50 (1996).
- Moritz, W. *et al.* Structure determination of the coincidence phase of graphene on Ru(0001). *Phys. Rev. Lett.* **104**, 136102–136105 (2010).
- Doniach, S. & Sunjic, M. Many-electron singularity in x-ray photoemission and x-ray line spectra from metals. *J. Phys. C* **3**, 285–291 (1970).
- Chen, H., Zhu, W. & Zhang, Z. Contrasting behavior of carbon nucleation in the initial stages of graphene epitaxial growth on stepped metal surfaces. *Phys. Rev. Lett.* **104**, 186101–186104 (2010).
- Knox, K. R. *et al.* Making angle-resolved photoemission measurements on corrugated monolayer crystals: Suspended exfoliated single-crystal graphene. *Phys. Rev. B* **84**, 115401–115413 (2011).
- Mavrikakis, M., Hammer, B. & Nørskov, J. K. Effect of strain on the reactivity of metal surfaces. *Phys. Rev. Lett.* **81**, 2819–2822 (1998).
- Vinogradov, N. A. *et al.* Formation and structure of graphene waves on Fe(110). *Phys. Rev. Lett.* **109**, 026101–026105 (2012).
- Stankovich, S. *et al.* Graphene-based composite materials. *Nature* **442**, 282–286 (2006).
- Diemant, T., Hager, T., Hoster, H., Rauscher, H. & Behm, R. Hydrogen adsorption and coadsorption with CO on well-defined bimetallic PtRu surfaces a model study on the CO tolerance of bimetallic PtRu anode catalysts in low temperature polymer electrolyte fuel cells. *Surf. Sci.* **541**, 137–146 (2003).
- Hoster, H. E. *et al.* Pt_xRu_{1-x}/Ru(0001) surface alloys formation and atom distribution. *Phys. Chem. Chem. Phys.* **10**, 3812–3823 (2008).
- Tanuma, S., Powell, C. J. & Penn, D. R. Calculations of electron inelastic mean free paths. II. data for 27 elements over the 50 ÷ 2000 eV range. *Surface and Interface Analysis* **17**, 911–926 (1991).
- Blöchl, P. E. Projector augmented-wave method. *Phys. Rev. B* **50**, 17953–17979 (1994).
- Perdew, J. P., Burke, K. & Ernzerhof, M. Generalized gradient approximation made simple. *Phys. Rev. Lett.* **78**, 1396–1396 (1997).
- Köhler, L. & Kresse, G. Density functional study of CO on Rh(111). *Phys. Rev. B* **70**, 165405–165413 (2004).
- Miniussi, E. *et al.* Thermal stability of corrugated epitaxial graphene grown on Re(0001). *Phys. Rev. Lett.* **106**, 216101–216104 (2011).

Acknowledgments

This work was sponsored by Italian Ministry for Research (MIUR), under the program PRIN2010-2011 grant 20105ZZTSE 'GRAF Frontiers in Graphene Research: understanding and controlling Advanced Functionalities'. D.A. and A.B. acknowledge the Royal Society for support. Calculations were run on the HECToR national facility in the U.K.

Author contributions

A.B. proposed and supervised the project; D.A. and M.P. carried out the density functional theory calculations; S.G., P.L., S.L. and R.L. provided the procedure for graphene preparation on bare Ruthenium; E.M., S.G., P.L., S.L., R.L. and A.B. carried out the photoemission spectroscopy measurements; E.M., B.S.B., T.O., A.L. and A.B. carried out the electron microscopy measurements; E.M. analysed the experimental data; E.M. and A.B. wrote the manuscript; all authors extensively discussed the results and commented on the manuscript.

Additional information

Supplementary information accompanies this paper at <http://www.nature.com/scientificreports>

Competing financial interests: The authors declare no competing financial interests.

How to cite this article: Alfè, D. *et al.* Fine tuning of graphene-metal adhesion by surface alloying. *Sci. Rep.* **3**, 2430; DOI:10.1038/srep02430 (2013).



This work is licensed under a Creative Commons Attribution-NonCommercial-NoDerivs 3.0 Unported license. To view a copy of this license, visit <http://creativecommons.org/licenses/by-nc-nd/3.0>